# A probabilistic approach to modeling microstructural variability and fatigue behavior in ASTM F562 medical grade wire

J. Schaffer*[1, 2]
[1]Fort Wayne Metals Research Products Corporation, USA; [2]Purdue University, USA
Jeremy_schaffer@fwmetals.com

*REFERENCE: Presented May 19th, 2006 at the 9th International Fatigue Congress, Atlanta, USA.*

**Abstract**

Several previous studies have demonstrated the importance of constituent inclusion particle distributions on variability in observed fatigue lifetimes. Such models have often concentrated on crack growth behavior in standard test specimens such as single edge notch tension (SENT) geometries. The methodology used here is similar to others in that constituent particles sizes were modelled as initial cracks that were grown to failure using a fracture mechanics approach. Lognormal distributions were fit to inclusion size parameters of 0.178 mm [0.007 in] ASTM F562 alloy medical grade wire. A critical volume approach was used to generate random subsets of inclusion sizes from which particles were chosen with a maximum likelihood of micro-crack generation. These sites were then grown at several stress levels to failure using a plasticity-induced crack-closure model to predict total fatigue life. The resulting lives were found to be in good general agreement with experimentally observed variability in rotary beam fatigue testing.

Keywords: crack growth, mp35n, 35n lt, medical wire, probabilistic fatigue

## Introduction

Medical appliances such as coronary lead implants, heart wall repair devices, and other long term implant technologies require the use of high strength, fatigue resistant and biocompatible wire materials to ensure adequate levels of performance. These devices are subsequently expected to endure the harsh biologic environment as long as the patient lives, often requiring the resistance to tens and even hundreds of millions of stress cycles due to patient movement, pulsatile stresses associated with vessel dilation/contraction, and a variety of other factors. A material of particular importance in coronary lead design is ASTM F562 by wt%, nominally a 35Co-35Ni-20Cr-10Mo alloy. ASTM F562 wire is used in low power bradycardia therapy pacing leads as the primary structural as well as electrical connection between the signal generator and target stimulation site and as a silver cored composite wire form in higher power defibrillation leads.

The fatigue process and its mechanisms are known to depend largely upon the presence of material inhomogeneities [1-4]. These may include intrinsic defects such as non-metallic inclusions, micropores, and grain boundaries, and extrinsic defects such as surface scratches and corrosion pits. This study focuses on cold drawn ASTM F562 wire, which is typically free of microporosity, possesses excellent corrosion resistance, and is drawn through diamond dies to yield an extremely smooth surface. The primary focus here is the growth of fatigue cracks from non-metallic inclusion sites contained within 35N LT®[1] and MP35N®[2] alloy. That is, two variants of specification ASTM F562 of significantly different microcleanliness whose average elemental assays are shown in Table 1.

## Material Background

MP35N was originally designed by SPS technologies as an aerospace fastener material specifically for the space shuttle [5]. The Co-Ni superalloy was designed to possess a high degree of toughness, corrosion resistance, and excellent cryogenic properties.

Table 1. Average wt% assay, MP35N and 35N LT

| Element | MP35N | 35N LT |
|---|---|---|
| Carbon | 0.010 | 0.010 |
| Manganese | 0.020 | 0.060 |
| Silicon | 0.040 | 0.030 |
| Phosphorus | 0.002 | 0.002 |
| Sulfur | 0.001 | 0.001 |
| Chromium | 20.45 | 20.58 |
| Nickel | 34.79 | 34.82 |
| Molybdenum | 9.52 | 9.51 |
| Iron | 0.44 | 0.52 |
| **Titanium** | **0.70** | **0.01** |
| Boron | 0.009 | 0.010 |
| Cobalt | Balance | Balance |

[1] 35N LT® is a registered trademark of Fort Wayne Metals Research Products Corp., IN, USA.
[2] MP35N® is a registered trademark of SPS Technologies, Jenkintown, PA.

It is this combination of properties in addition to its remarkable resistance to fatigue damage that have bolstered its use in the medical device industry in the past twenty years. This transition to medical service has also made known some weaknesses in the conventional alloy system. At the micro length scales associated with fine medical wire, the intrinsic constituent titanium nitride (TiN) particle content of MP35N has been shown to be a significant detriment to total fatigue life [4]. In the 35N LT alloy system, the small addition of titanium (<1 wt%) in MP35N for melt deoxidation was replaced with magnesium. The result of this modification was a reduction in typical transverse inclusion sizes from ~ 10 – 20 μm to less than 3 μm. As shown in Fig. 1, the resultant magnesium oxide (MgO) inclusions were found to possess a near spherical morphology in contrast to the sharp cubic structure associated with TiN.

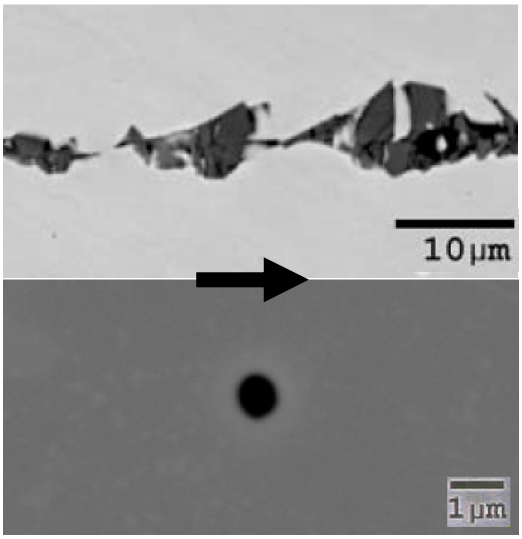


Fig. 1. Backscattered electron image (BEI) of a typical inclusion found in MP35N (top), BEI of a typical 35N LT inclusion feature (bottom); arrow indicates longitudinal wire drawing direction

**Material Processing & Properties**

Both materials used for this investigation were initially cast into 1360 kg [3000 lb] vacuum induction melt (VIM) electrodes which were vacuum arc remelted (VAR) into 432 mm [17 in.] diameter ingots. After a homogenization treatment, the VAR ingots were reduced on a rotary forge (GFM) machine to produce 100 mm [4 in.] diameter billet which was subsequently hot rolled on a continuous rolling mill to 5.6 mm [0.219 in.] diameter coil. The coil was annealed, shaved to 5.5 mm [0.216 in.] and pickled in preparation for drawing. Intermediate reduction from 5.5 mm to 1.6 mm [0.064 in.] was accomplished using carbide drawing dies and powder lubricants. Additional processing to the final diameter of 0.178 +/- 0.005 mm [0.007 +/- .0002 in.] was completed using diamond dies and mineral oil lubricants. A qualitative comparison between the surface characteristics of each material was performed using scanning electron microscopy (SEM). Generally, the 35N LT was found to possess a more uniform surface due to fewer and smaller intrinsic surface defects (see Fig. 2). These findings were consistent with results reported by Kay *et al.,* in ref. [4].

Three nominal strength levels were targeted for evaluation: a 1310 MPa [190 ksi] ultimate tensile strength (UTS) annealed specimen possessing an equiaxed grain structure, material strain hardened to 1930 MPa [280 ksi] UTS, and a final sample at 2206 MPa [320 ksi] UTS. The latter two samples were selected for their applicability to use within the medical device field, particularly for use in implantable lead design. The equiaxed structure was selected in order to study the expected growth and arrest of short fatigue cracks at grain boundaries. Cold drawing ASTM F562 wire results in a multiphase reaction comprising a strain-induced crystallographic transformation from annealed parent face-centered-cubic (FCC) to hexagonal-close-packed (HCP) structure [5]. This transformation makes discernment of original grain boundaries difficult. Measured material tensile properties were found to be comparable for both alloys and are shown in table 2.

Table 2. Tensile properties* of 0.178 mm ASTM F562 wire materials

| Sample ID | YS [MPa] | UTS [MPa] | %Elongation |
|---|---|---|---|
| MP35N-1310 | 876 | 1262 | 35.0 |
| 35N LT-1310 | 924 | 1289 | 35.0 |
| MP35N-1930 | 1600 | 1889 | 4.00 |
| 35N LT-1930 | 1710 | 1889 | 3.60 |
| MP35N-2206 | 1696 | 2158 | 2.80 |
| 35N LT-2206 | 1813 | 2158 | 2.80 |

**Tests were conducted on an Instron model 4469 system using a 1000 N load cell, 10 inch gage length, and a cross head speed of 5 inch/minute*

**Deterministic Crack Growth Model**

Newman *et al.,* have successfully demonstrated the use of a deterministic fatigue crack growth model as applied to aluminum and titanium alloys, as well as to high strength 4340 steel [6]. Newman's FASTRAN II [17,18] computer program utilizes a plasticity-induced crack-closure scheme to predict fatigue lives of metallic materials. The incorporation of crack tip plasticity and crack closure effects is a proposed method of dealing with the nonlinearities associated with relatively high stress-intensity factors, low-cycle fatigue conditions and transitional crack growth from

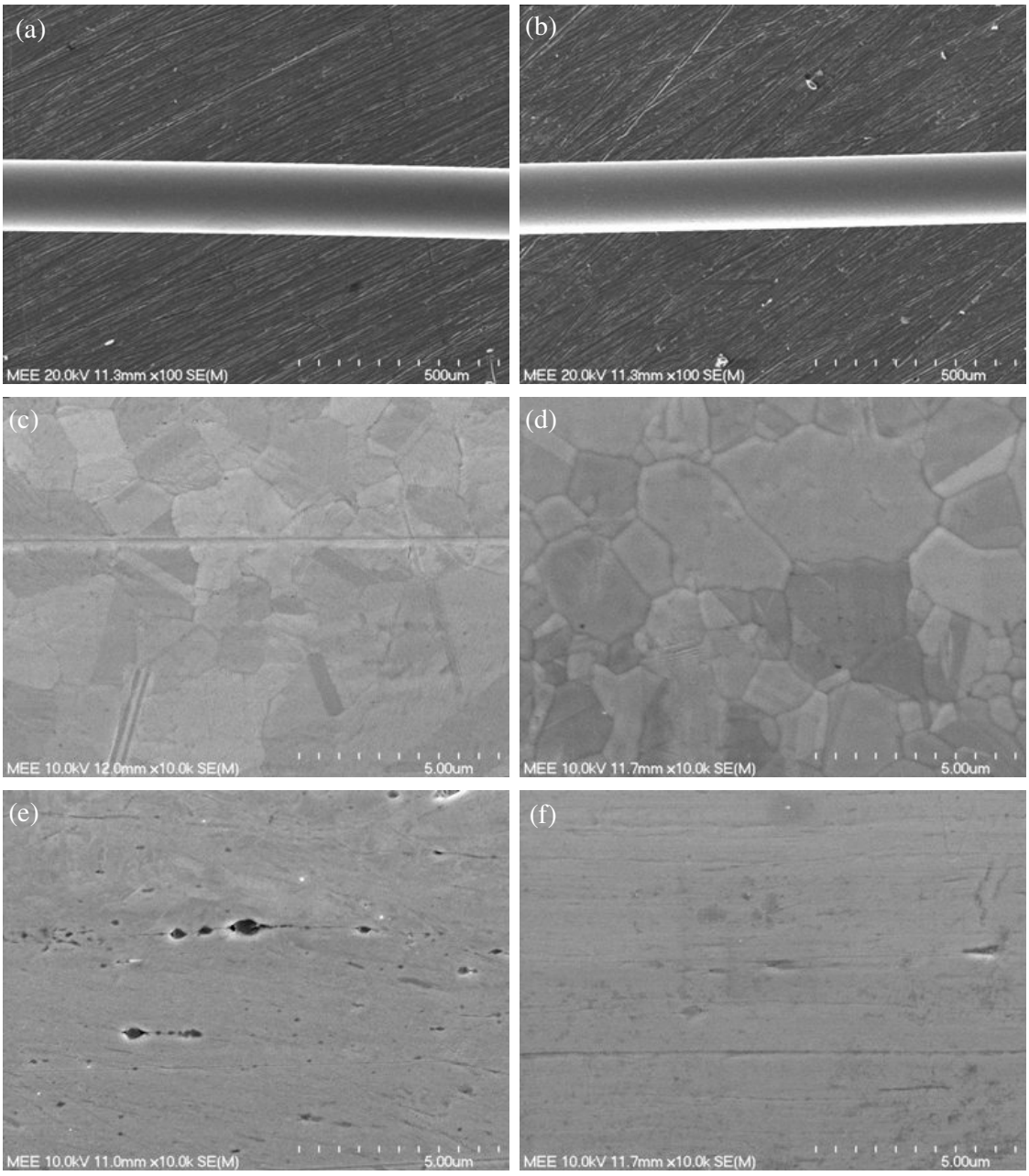


Fig. 2. Material surface comparison. (a) Original magnification 100 X, SEI image of UTS 1930 MPa, MP35N and (b) 35N LT exhibiting overall smooth, diamond drawn surface. (c) Original magnification 10 kX, SEI image of UTS 1310 MPa annealed MP35N with light die line; (d) 35N LT with visible surface grain boundaries. (e) Original magnification 10 kX, BEI image of UTS 2206 MPa MP35N with characteristic TiN inclusion stringer and (f) 35N LT with smooth, inclusion free surface.

microstructurally small initiation sites. The program calculates the stress at which the crack is fully opened ($S_o'$) and incorporates this into a cyclic-plastic-zone-corrected effective stress-intensity factor range given by

$$\Delta K_{eff} = (S_{\max} - S_o')\sqrt{\pi d}\, F(d/w) \qquad (1)$$

where $S_{max}$ is the maximum applied stress, $S_o'$ is the crack opening stress, d is the current crack length plus the crack growth rate (dc/dN) for one cycle and F is the cyclic-plastic-zone corrected boundary correction factor which may be a function of several geometric configuration parameters including width, thickness or notch radius.

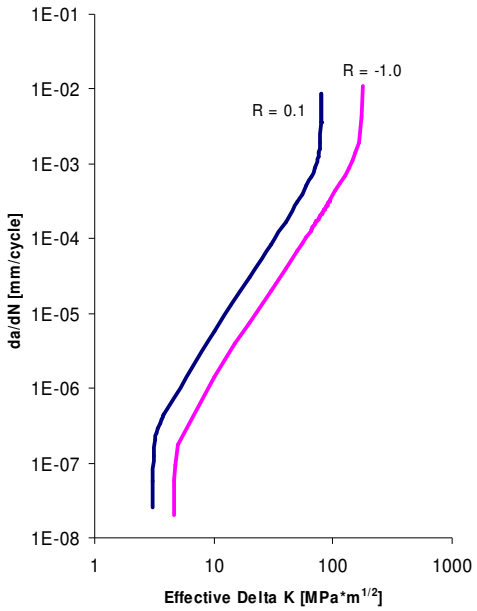


Fig. 3. Crack growth data for MP35N adapted from ref. [11].

Optimally, crack growth data for the deterministic model should be obtained for a given set of parameters including: surface condition, grain size, load situation, crack propagation direction, and others. In the case of highly anisotropic fine wire, very little data is available in the literature on crack growth behavior. For this reason, the initial step in research used the data shown in Fig. 3, taken using a standard three-point-bend [SE(B)] fracture specimen. The data was adapted for R = -1 testing according to equation 2,

$$\frac{da}{dN} = \frac{C(1-f)^n \Delta K^n \left(1 - \frac{\Delta K_{th}}{\Delta K}\right)^p}{(1-R)^n \left(1 - \frac{\Delta K}{(1-R)\Delta K_c}\right)^q} \qquad (2)$$

where:

N = number of cycles
a = crack length
ΔK = stress intensity factor range
$\Delta K_{eff}$ = effective stress intensity factor range
C,n,p,q = empirically defined constants (Table 3)
f = crack opening function for plasticity-induced closure

Table 3. Crack growth constants for MP35N

| Equation 2 constant | Curve fit value |
|---|---|
| C | 5.410 E-08 |
| n | 2.280 |
| P | 0.250 |
| q | 0.250 |

Total fatigue life in the deterministic model is represented entirely as a propagation process beginning from an input microstructural flaw or equivalent flaw size and through small and large crack growth regimes [2]. Such a model does not account for occasional crack arrest due to microstructural variation such as high angle grain boundaries, and acceleration due to dislocation pileup stress intensification associated with other boundary interactions. In other studies [2, 3, 7-9], however; the model has well predicted critical shorter lives resulting from large tail distribution initiation sites. From a designer's perspective, it is these shorter lives that are of most concern, thus lending significant value to such a tool.

**Probabilistic Model**

Many approaches have been employed in an effort to predict fatigue life from known statistical distributions of constituent particles. Laz *et al.* [6] successfully developed a probabilistic total fatigue life model for 2024-T3 Aluminum in which cracked particles were shown to be the dominant crack nucleation sites. Sharpe *et al.* [3] followed a similar probabilistic methodology and generated robust predictive results in AISI 4340 high strength steel. The majority of previous studies have focused on the use of standard test geometries, such as single edge notch tension (SENT) specimens. One primary objective of this research is to demonstrate the applicability of such modeling techniques in a non-standard geometry, one that is more suited to use in a finished medical device.

The deterministic crack growth model assigns a unique life in a given material for each equivalent initial flaw size that is input as the growth starting point. The advantage of combining a probabilistic approach with the deterministic growth model is that a complete life and life variability prediction may be made through knowledge of material heterogeneity size distributions. The probabilistic model used here is similar to the one developed by Laz and Hillberry in ref. [3].

Advances in electron microscopy and image analysis tools have made characterization of microcleanliness a straight forward and cost effective exercise. The value of such information is significantly enhanced if one can make predictions concerning the material's total fatigue life and life variability in various geometries, stress conditions and strain hardening states. SEM, digital image

analysis, and energy dispersive spectroscopy (EDS) were employed here in order to fully characterize the statistical size distribution, inclusion particle shape, and particle chemistry. Flaw size distributions were surveyed and compared in both 2.5 mm diameter material as well as in the final size 0.178 mm diameter wire and found to be relatively similar in terms of transverse inclusion size as shown in Fig. 4.

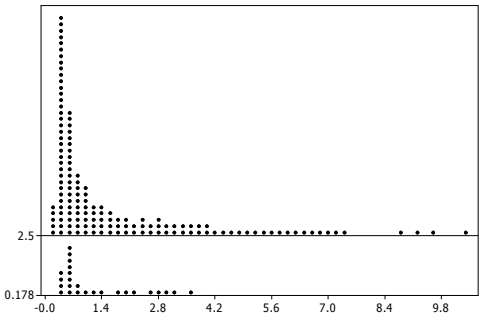


Fig. 4. Frequency dot plot showing similarity between transverse TiN inclusion size (μm) distributions in MP35N wire for 2.5 mm [top, N=4103] and 0.178 mm [bottom, N=484] wire.

As represented in Fig. 5, the distribution of the inclusions with respect to volume was found to be essentially uniform in both sizes and material systems examined. The finding of volumetric uniformity was somewhat surprising considering the amount of cold deformation and increase in surface area imparted to the wire during the drawing operation. Such operations have been theorized to yield a relative drift in the radial position of hard inclusion particles. The cumulative distribution function (CDF) of radial position for the 0.178 mm wire shown in Fig. 6 confirms the finding that the constituent particle uniformity associated with the homogenizing VIM / VAR melt practice has survived all the way to fine diameter wire.

The findings of volumetric uniformity are important because they support the use of intrinsic constituent particle data collected at large starting sizes to predict fatigue performance of finished fine wire parts. The CDF of a given wire cross section, assuming volumetric uniformity would be given by the area ratio at a given radius divided by the wire area or,

$$\text{F(R) = P(particle contained in R)} = \left(\frac{R}{R_w}\right)^2 \qquad (3)$$

where P is the probability of finding an inclusion within R, R is the inner radius and $R_w$ is the wire radius as shown in Fig. 5.

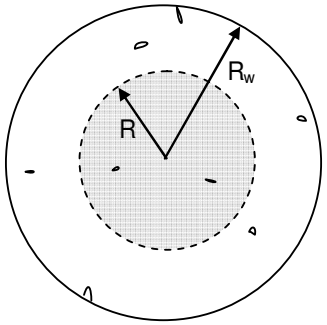


Fig. 5. Volumetric inclusion distribution uniformity description

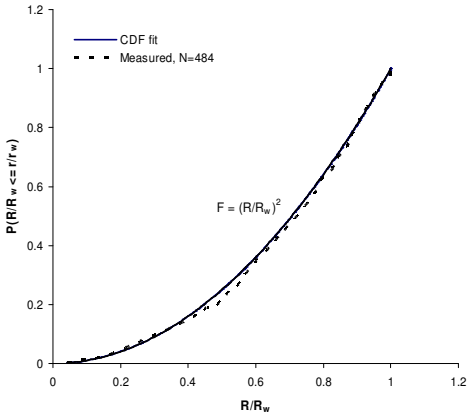


Fig. 6. Radial inclusion distribution, representative of findings in both MP35N and 35N LT

Determination of the inclusion content in relatively large materials, such as the 2.5 mm wire examined in this study, is a relatively simple task. In this case, 160 images were collected at 1000 X magnification from random MP35N wire sections using backscattered electron imaging (BEI) in an SEM for a total examined area of 1.73 $mm^2$ of transverse wire area. This was repeated for three materials lots yielding a total number of inclusions counted of 4103. The image data was then analyzed using digital processing to yield information for inclusion length, breadth, area, aspect ratio, and radial position. Similar analysis of three lots of 2.5 mm 35N LT yielded a total of 722 particle sites. The resultant geometric parameters were then empirically fit to CDF's using lognormal fitting functions. The results of this analysis are shown in Fig. 7 – 10.

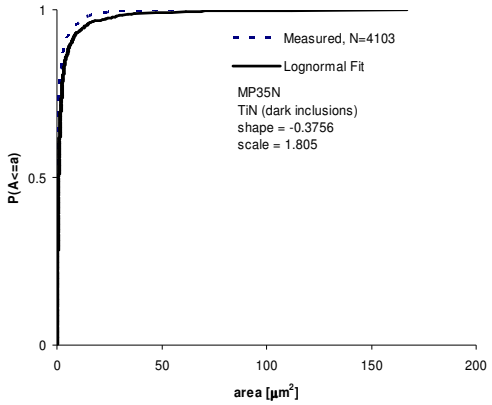


Fig. 7. Inclusion area distribution for 2.5 mm MP35N wire

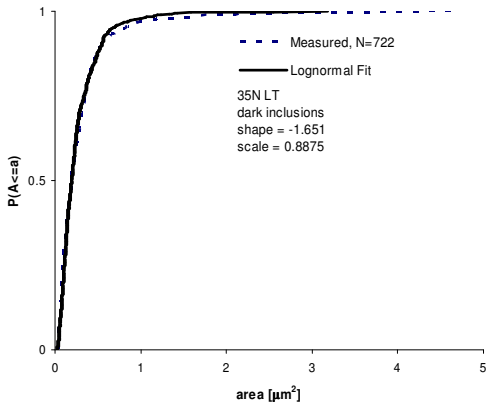


Fig. 8. Inclusion area distribution for 2.5 mm 35N LT wire

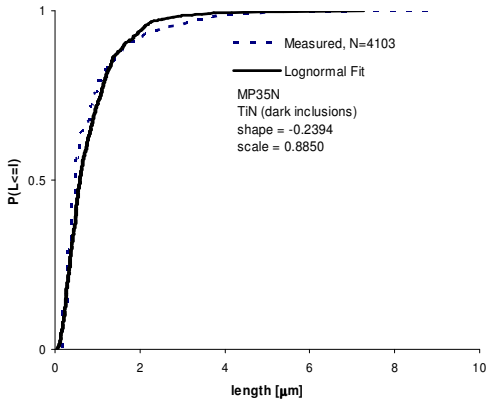


Fig. 9. Inclusion breadth distribution for 2.5 mm MP35N wire

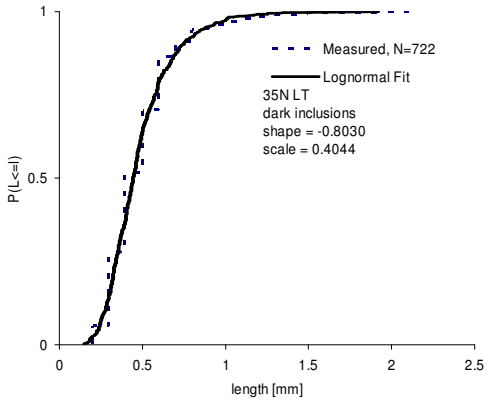


Fig. 10. Inclusion breadth distribution for 2.5 mm 35N LT wire

Inclusion content determination of the 0.178 mm wire was more time consuming due to the large number of cross sections that had to be examined. As shown in Fig. 11, nineteen wire strand bundles of the fine diameter wire were used to cut down on the amount of time spent mounting individual wire sections. The bundling was performed using a minimal pitch angle of just several degrees in order to reduce the impact of cross sectional distortion. The organization associated with the *1x19* wire bundles also yielded excellent reference points for the automated image analysis post processing.

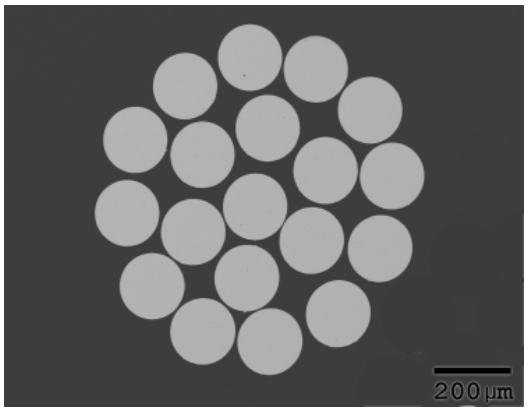


Fig. 11. Nineteen wire bundle used for inclusion analysis of 0.178 mm wire.

As discussed, typical inclusion findings in standard MP35N wire comprise cubic titanium nitride (TiN) particles, while the common particles in 35N LT are composed of generally spherical magnesium oxide (MgO) particles. Representative images of inclusions found in this survey and an energy dispersive spectrum (EDS) of a TiN particle are shown in Fig. 12, 13, and 14 respectively.

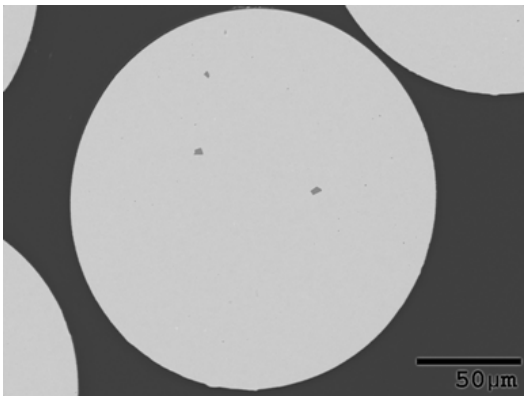


Fig. 12. SEM BEI image of a 0.178 mm wire cross section of MP35N wire showing a typical distribution of TiN constituent inclusions particles

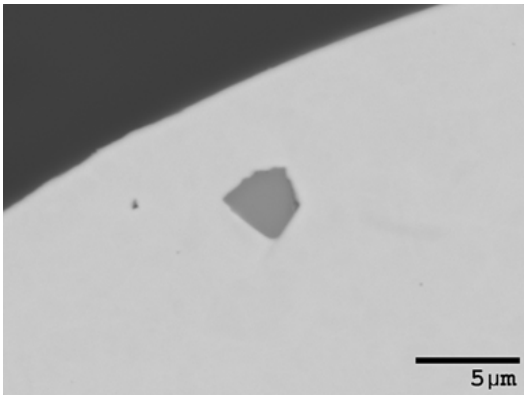


Fig. 13. SEM BEI image of a near-surface TiN particle in MP35N

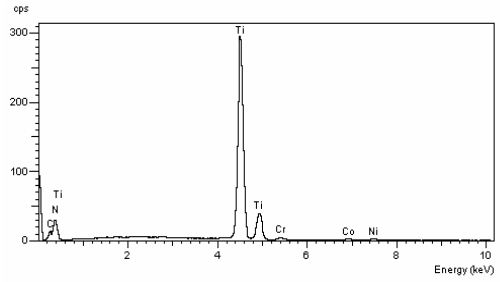


Fig. 14. Typical energy dispersive spectra results for a TiN inclusion in MP35N

## Residual Stress Distribution

Ideal SENT, single edge notch bending SE(B) and other standard crack geometries are often carefully machined and/or chemically prepared so that they are free from machining induced residual stresses, grooves and other factors that may influence fatigue behavior. Seldom, in real world medical devices, is such preparation practical or even feasible. Wire that is cold drawn through carefully designed die profiles to obtain high mechanical strength will unfailingly contain a non-zero residual stress distribution. Most commonly, wire draw processing will leave a crack opening residual tensile stress at the surface and a compressive stress near the wire's centerline. In this study, wire samples were sent to Lambda Technologies for X-ray diffraction analysis in order to characterize residual stresses in the 0.178 mm MP35N and 35N LT wires. The results of the residual stress determination are presented in Fig. 15 and 16.

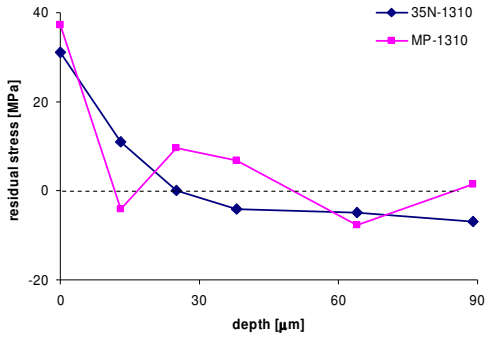


Fig. 15. Residual stress distribution in annealed wire samples, note that 88.9 □m depth represents the wire centreline.

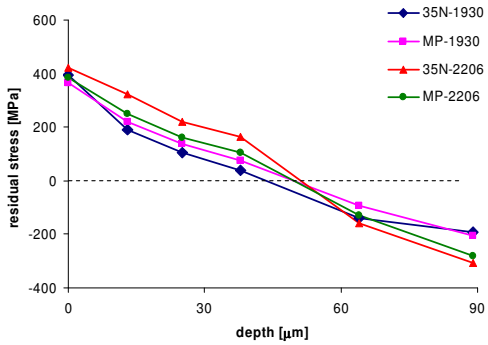


Fig. 16. Residual stress distribution in cold-drawn wire samples showing consistency between alloys and strain hardening states.

## Results & Conclusions

The primary purpose of this paper was to explore a probabilistic method of microstructural characterization coupled to a deterministic fatigue crack growth model in order to predict 1) total fatigue life and 2) fatigue life variability of fine medical grade wire. While this research is an ongoing project, the current findings with respect to life prediction certainly look promising. To demonstrate the power of such a model, inclusion sizes from the lognormal distributions given herein for MP35N wire were input randomly into the non-linear FASTRAN II growth model in conjunction with the crack growth rate data taken from the

SE(B) geometry of ref. [11] and fracture toughness given in ref. [10]. This data was applied with an implicitly defined ΔK threshold of 4.65 MPa(m)$^{1/2}$. CDF plots at two stress levels of 1030 and 1380 MPa (Fig. s 17 and 18 respectively) with a stress ratio of R = -1 were produced and compared to experimental results obtained from rotary bend fatigue testing (RBT) of the 1930 MPa samples. Considering the crack growth data was derived from a completely different material form, vintage and melt source, the results seem surprisingly good. This is indicative of the robustness of the plasticity-induced-closure model used in the FASTRAN growth scheme developed by Newman.

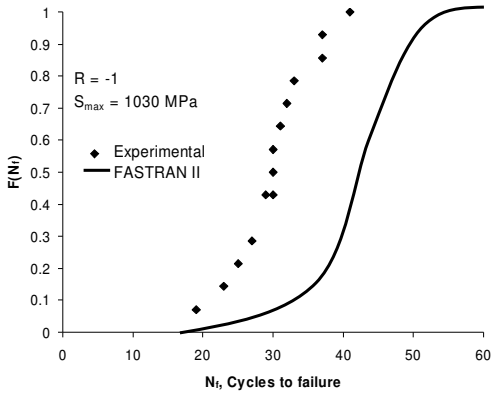


Fig. 17. CDF results for 0.178 mm fatigue testing at S = 1030 MPa, R=-1 conditions.

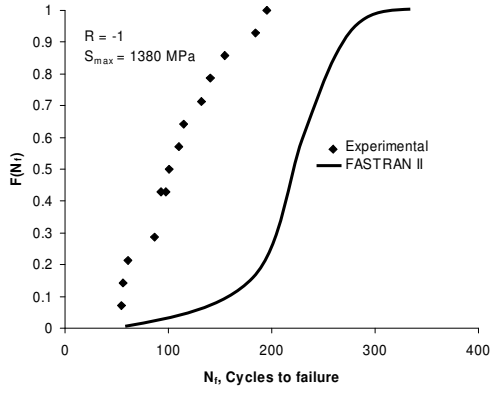


Fig. 18. CDF results for 0.178 mm fatigue testing at S = 1380 MPa, R=-1 conditions.

In this preliminary stage of research, the full inclusion distribution was used as input for the fatigue crack growth (FCG) model. However, it is known that the majority of smaller inclusions will not necessarily initiate fatigue cracks and that it is the large tail that will likely be responsible for the vast majority of crack initiation sites [2,3,7-9,12,15]. This is also the likely reason that the current model yielded a non-conservative CDF result for both stress levels considered. As this research continues, emphasis will be placed on better understanding the crack nucleating (CN) inclusion distributions and perhaps use of a similar probability of crack nucleation (POCN) transformation to that used by Laz and Hillberry in ref. [2].

## Acknowledgements

The author gratefully acknowledges funding provided by Fort Wayne Metals Research Products, Fort Wayne, IN in making possible this research. In addition, a special thanks goes out to Materials Evaluation & Engineering (MEE) for their continued excellence in materials analysis techniques.

## References

[1] Shenoy, M.M., Kumar, R.S. and McDowell D.L. Modeling effects of nonmetallic inclusions on LCF in DS nickel-base superalloys. *International Journal of Fatigue*, 2005, 27:113-127.

[2] Laz, P.J., Craig, B.A. and Hillberry, B.M. A probabilistic total fatigue life model incorporating material inhomogeneities, stress leval and fracture mechanics. *International Journal of Fatigue*, 2001, 23:119-127.

[3] Laz, P.J. and Hillberry, B.M. Fatigue life prediction from inclusion initiated cracks. *International Journal of Fatigue*, 1998; 20:263-70.

[4] Bradley, D. and Kay, L. Optimization of Melt Chemistry and Properties of 35Cobalt-35Nickel-20Chromium-10Molybdenum Alloy Medical Grade Wire. *ASM M&PMD Conference Proceedings*, 2003:336-343.

[5] Superalloys Developed by SPS Technologies for Aerospace Fasteners. SPS Technologies Technical Literature, SPS Technologies, Jenkintown, PA, 1998:1-16.

[6] Newman, J.C., Phillips, E.P., and Swain, M.H. Fatigue-life prediction methodology using small-crack theory. *International Journal of Fatigue*, 1997; 21:109-119.

[7] Sharpe, P.S., Hillberry, B.M., and Craig, B.A., Fatigue Life Variability Prediction Based on Crack Forming Inclusions in a High Strength Alloy Steel. *Probabilistic Aspects of Life Prediction, ASTM STP 1450*, W.S. Johnson and B.M. Hillberry, Eds., ASTM International, West Conshohocken, PA, 2003.

[8] DeBartolo, E.A. and Hillberry, B.M. A model of initial flaw sizes in aluminium alloys. *International Journal of Fatigue*, 2001; 23:79-86.

[9] DeBartolo E.A. and Hillberry, B.M., Effects of constituent particle clusters on fatigue behavior of 2024-T3 aluminum alloy. *International Journal of Fatigue*, 1998; 20(10):727-735.

[10] Shaji, E.M., Kalidindi, S.R., *et al.,* Fracture properties of multiphase alloy MP35N. *Materials Science and Engineering*, 2003; A349:313-317.

[11] Henkener, J.A., Lawrence, V.B., and Forman, R.G., An evaluation of fracture mechanics properties of various aerospace materials. *Fracture Mechanics: Twenty-Third Symosium, ASTM STP 1189,* Ravinder Chona, Ed., American Society for Testing and Materials, Philadelphia, 1993; 474-497.

[12] Bjerken, C., The discrete nature of the growth and arrest of microstructurally short fatigue cracks modelled by dislocation technique. *International Journal of Fatigue*, 2005; 27(1):21-32.

[13] Trantina, G.G. and Barishpolsky, M., Elastic-plastic analysis of small defects voids and inclusions. *Engineering Fracture Mechanics*, 1984; 20(1):1-10.

[14] Marrey, R.V. *et al.*, Fatigue and life prediction for cobalt-chromium stents: A fracture mechanics analysis. *Biomaterials at sciencedirect.com*, 2005; 1-13.

[15] Mercer, C., Soboyejo, A.B.O., Soboyejo, W.O., Micromechanisms of fatigue crack growth in a forged Inconel 718 nickel-based superalloy. *Materials Science and Engineering*, 1999; A270:308-322.

[16] Pugno, N., Ciavarella, M., Cornetti, P., and Carpinteri, A., A generalized Paris' law for fatigue crack growth. *Journal of the Mechanics and Physics of Solids*, 2006; 54(7):1333-1349.

[17] Newman, J.C., Jr, Phillips, E.P., Swain, M.H. and Everett, R.A., Jr, Fatigue mechanics: an assessment of a unified approach to life prediction. *Advances in Fatigue Lifetime Predictive Techniques,* ASTM STP 1122, eds. M.R. Mitchell and R.W. Ladngraf, American Society for Testing and Materials, Philadelphia, 1992, pp. 5-27.

[18] Newman JC Jr. Fastran II – a fatigue crack growth structural analysis program. NASA-TM-104159, Hampton (VA): NASA Langley Research Center, 1992.